Supplementary Information for

Modulating Adsorbed Hydrogen Drives Electrochemical CO_2-to-C_2 Products

Jiaqi Feng, Libing Zhang, Shoujie Liu, Liang Xu, Xiaodong Ma, Xingxing Tan, Limin Wu, Qingli Qian, Tianbin Wu, Jianling Zhang, Xiaofu Sun*, Buxing Han*

Supplementary Figures and Tables

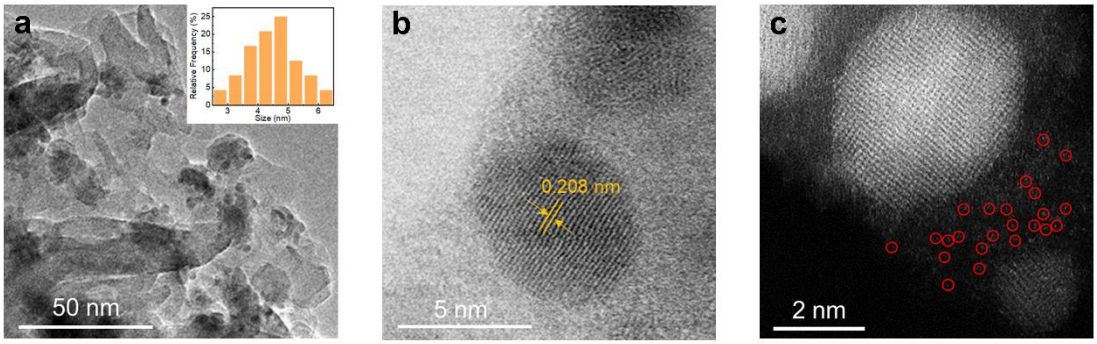

Figure S1. (a) TEM image (inset shows particle size distribution), (b) HRTEM image and (c) aberration-corrected HAADF-STEM image of P-Cu_1/Cu_{NP}.

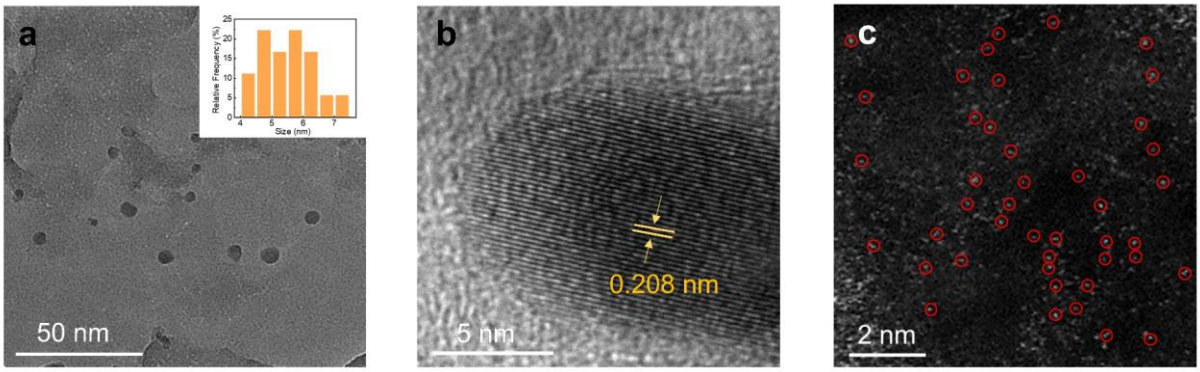

Figure S2. (a) TEM image (inset shows particle size distribution), (b) HRTEM image and (c) aberration-corrected HAADF-STEM image of R-Cu_1/Cu_{NP}.

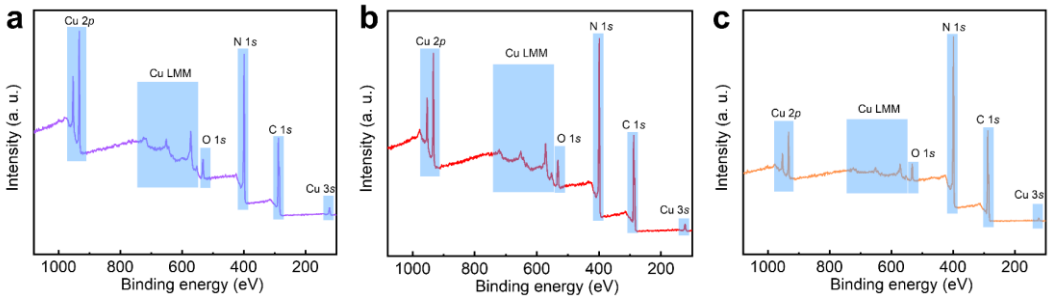

Figure S3. XPS survey spectra of (a) P-Cu_1/Cu_{NP}, (b) M-Cu_1/Cu_{NP} and (c) R-Cu_1/Cu_{NP}.

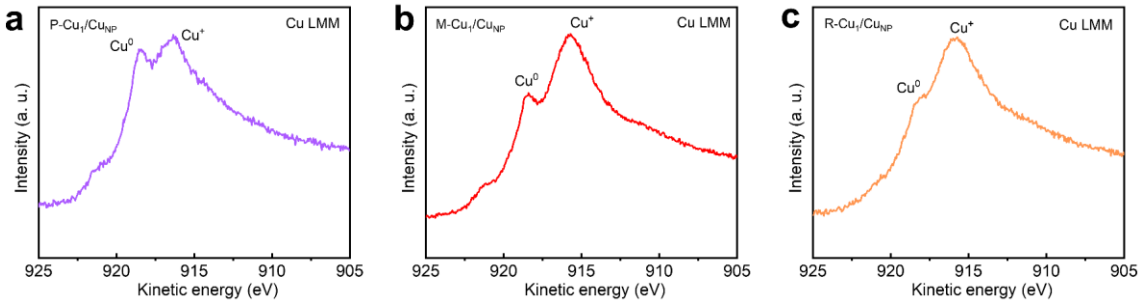

Figure S4. Cu Auger LMM spectra of (a) P-Cu_1/Cu_{NP}, (b) M-Cu_1/Cu_{NP} and (c) R-Cu_1/Cu_{NP}.

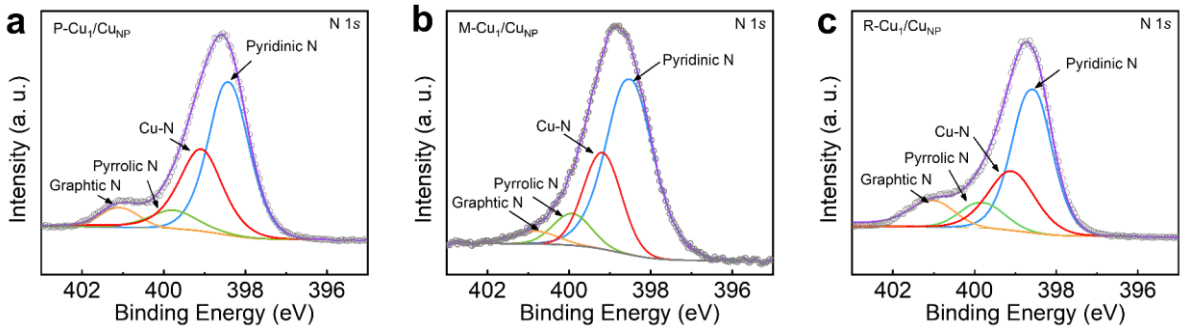

Figure S5. XPS spectra of N 1*s* orbits of (a) P-Cu_1/Cu_{NP}, (b) M-Cu_1/Cu_{NP}, and (c) R-Cu_1/Cu_{NP}.

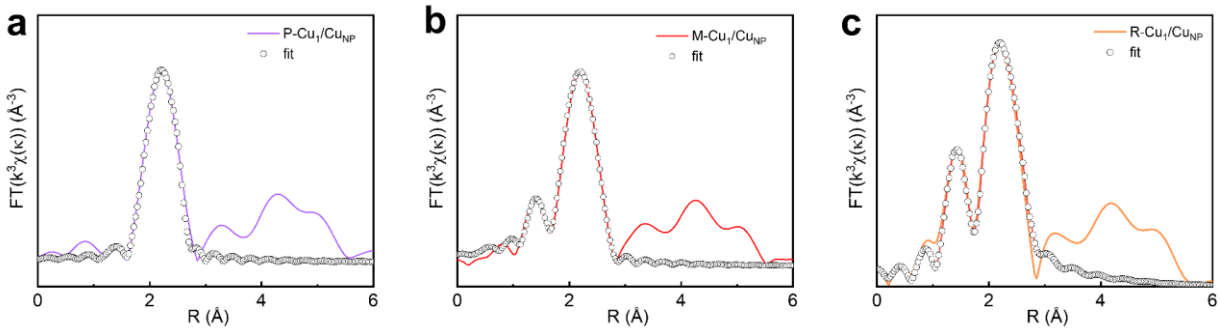

Figure S6. Least-squares EXAFS fittings of (a) P-Cu_1/Cu_{NP}, (b) M-Cu_1/Cu_{NP}, and (c) R-Cu_1/Cu_{NP}.

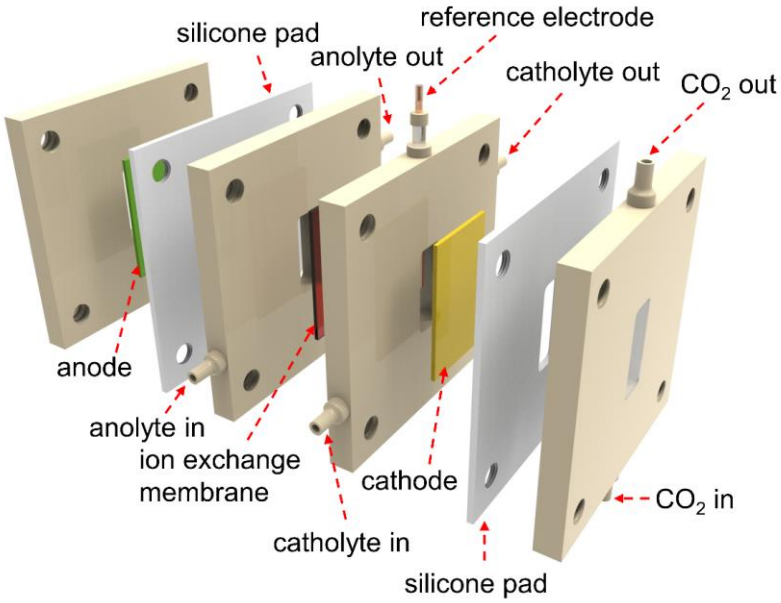

Figure S7. The scheme of flow cell used for CO_2RR tests.

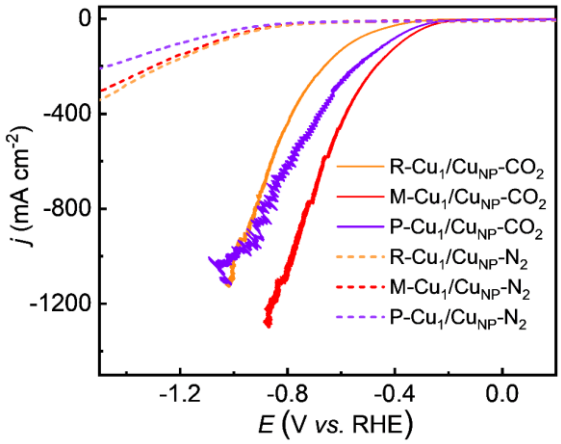

Figure S8. LSV curves of R-Cu_1/Cu_{NP}, M-Cu_1/Cu_{NP} and P-Cu_1/Cu_{NP} in CO_2 or N_2 atmosphere, the experiments were performed in 5 M KOH electrolyte with 20 mV s^{-1} scan rate and 80% ohmic compensation.

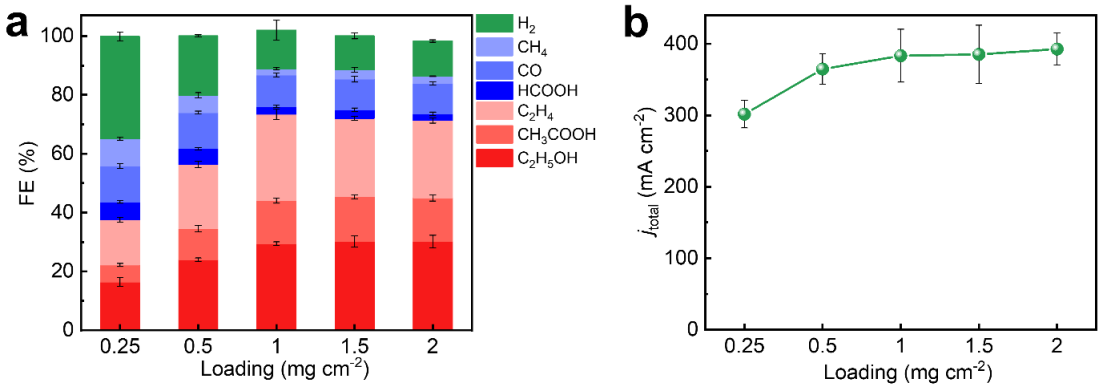

Figure S9. (a) Product FEs and (b) current density of M-Cu_1/Cu_{NP} at -0.6V in 5 M KOH electrolyte with various catalyst loading. Both C_2 products selectivity and total current density increased as the increasing loading of M-Cu_1/Cu_{NP} until 1 mg cm^{-2}, and no obvious difference was observed among 1, 1.5 and 2 mg cm^{-2}. Therefore, we chose 1 mg cm^{-2} as the catalyst loading to conduct activity experiments.

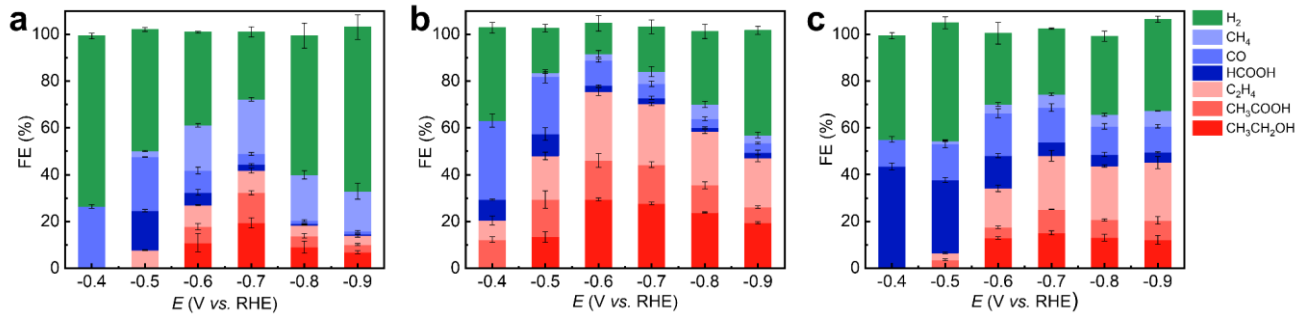

Figure S10. The CO_2RR prodcuct FEs of (a) R-Cu_1/Cu_{NP}, (b) M-Cu_1/Cu_{NP} and (c) P-Cu_1/Cu_{NP} under different applied potentials, the experiments were performed in 5 M KOH electrolyte with 80% ohmic compensation. Values are means and error bars indicate s.d. (n = 3 replicates).

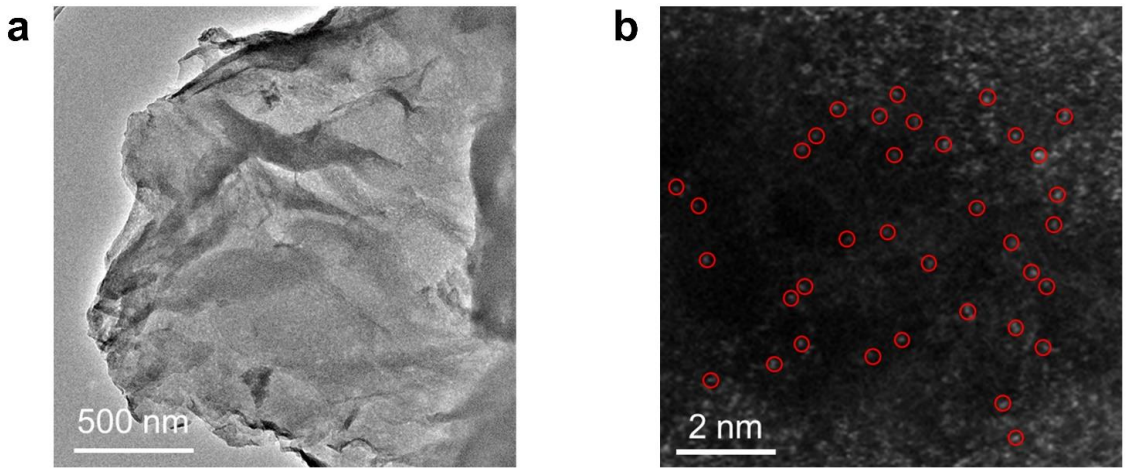

Figure S11. (a) TEM and (b) aberration-corrected HAADF-STEM images of Cu-N-C. The Cu-N-C was obtained by acid treatment of M-Cu_1/Cu_{NP}: the M-Cu_1/Cu_{NP} was added into 50 mL 1 M sulfuric acid aqueous solution and heated at 80 °C for 48 h, then washed with deionized water several times and dried at 80°C overnight.
No obvious nanoparticles were observed in TEM image and a large amount of isolated bright dots recognized as Cu single atoms were observed in aberration-corrected HAADF-STEM image.

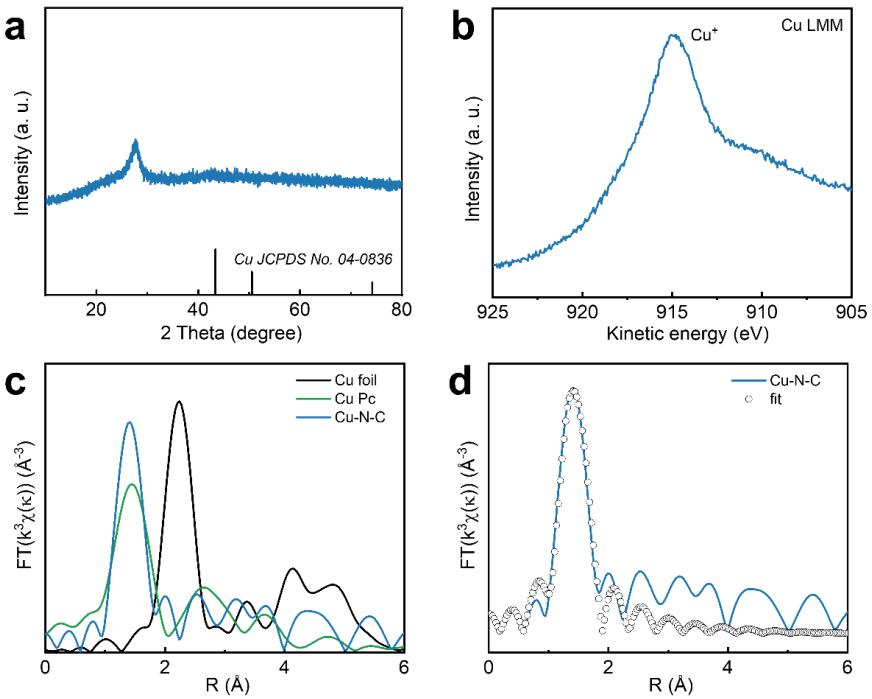

Figure S12. (a) XRD pattern, (b) Cu Auger LMM spectrum, (c) EXAFS spectra, and (d) least-squares EXAFS fittings of Cu-N-C. The Cu-N-C was obtained by acid treatment of M-Cu_1/Cu_{NP}: the M-Cu_1/Cu_{NP} was added into 50 mL 1 M sulfuric acid aqueous solution and heated at 80 °C for 48 h, then washed with deionized water several times and dried at 80°C overnight.

No diffraction peaks related to crystalline Cu species can be identified in XRD pattern. XPS spectra showed that Cu element existed in Cu-N-C catalyst and Cu^+ was main specie. More importantly, the EXAFS profiles in the R-space of Cu-N-C suggested that only the peak attributed to Cu-N coordination located at around 1.4 Å, while the Cu-Cu coordination peak at around 2.2 Å disappeared, which confirmed that the Cu species only existed as single atom form. The results of least-squares EXAFS fitting confirmed that the Cu-N coordination numbers in Cu-N-C was 4.0 (Table S2), implying that the atomic Cu species mainly existed as $Cu-N_4$ structure.

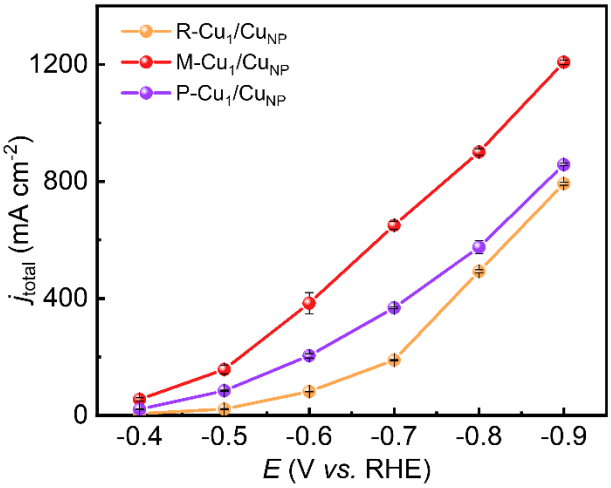

Figure S13. Total current density of R-Cu_1/Cu_{NP}, M-Cu_1/Cu_{NP} and P-Cu_1/Cu_{NP} at different applied potentials in 5 M KOH electrolyte. Values are means and error bars indicate s.d. (n = 3 replicates).

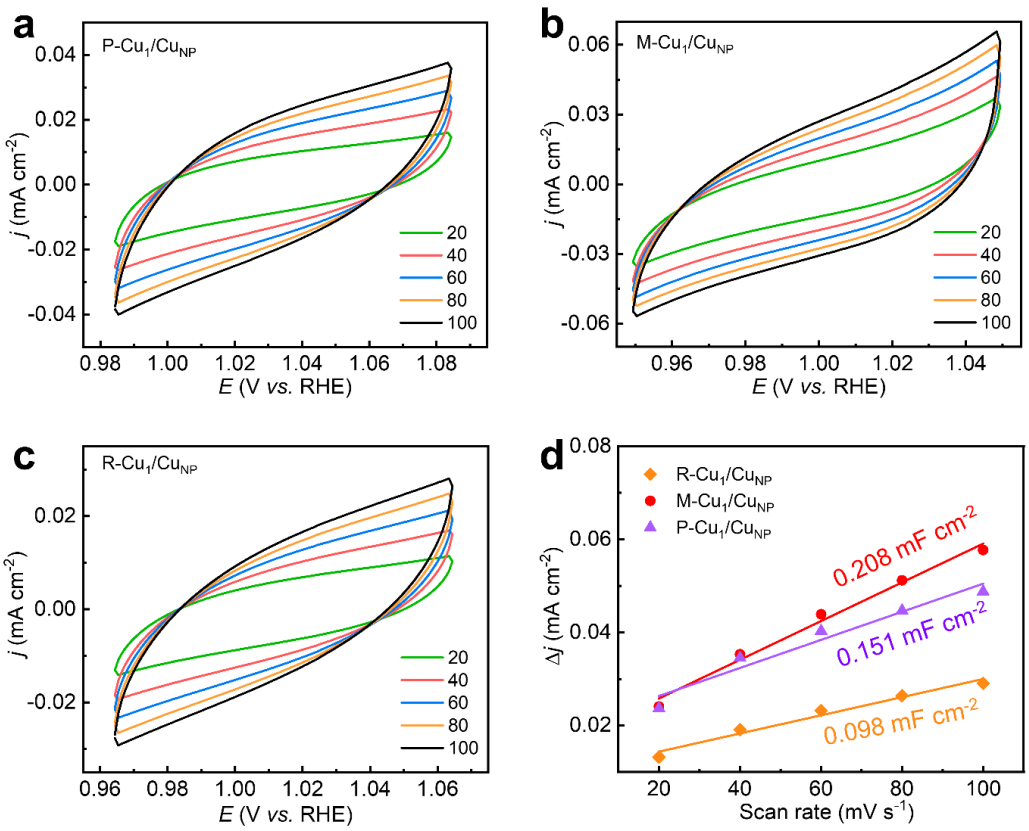

Figure S14. Cyclic voltammograms with different scan rates (20, 40, 60, 80, 100 mV s^{-1}) for (a) P-Cu_1/Cu_{NP}, (b) M-Cu_1/Cu_{NP}, and (c) R-Cu_1/Cu_{NP} in 0.5 M $KHCO_3$ electrolyte. (d) Linear fitting of double-layer capacitive currents Δj versus scan rate.

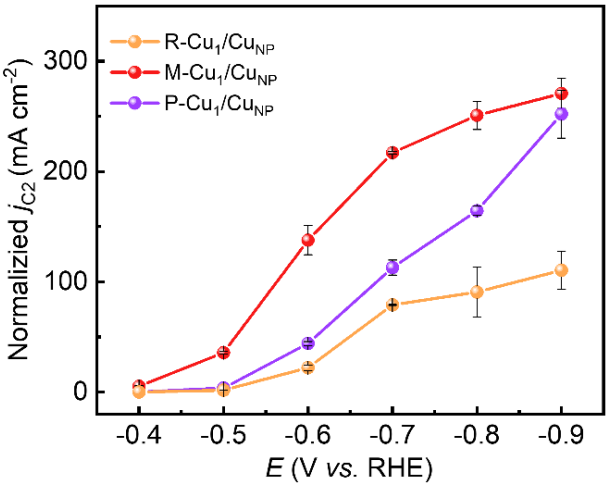

Figure S15. The j_{C2} of R-Cu_1/Cu_{NP}, M-Cu_1/Cu_{NP} and P-Cu_1/Cu_{NP} after normalized by ECSA in 5 M KOH electrolyte.

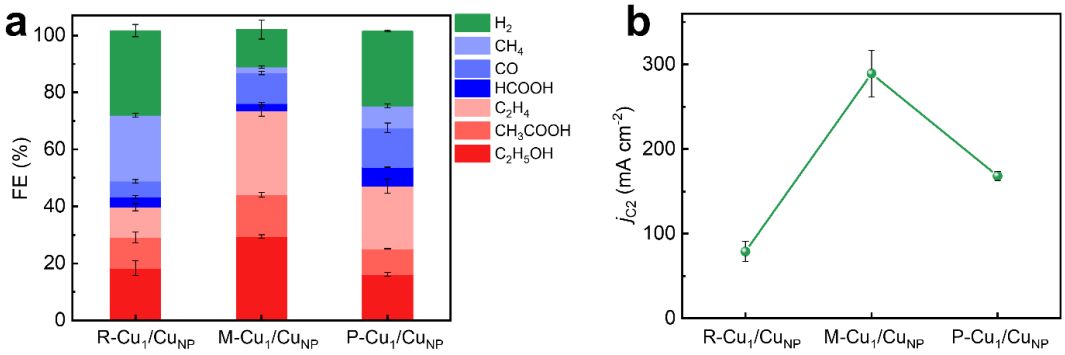

Figure S16. The (a) products FE and (b) j_{C2} of R-Cu_1/Cu_{NP}, M-Cu_1/Cu_{NP} and P-Cu_1/Cu_{NP} under similar ECSA condition in 5 M KOH electrolyte.

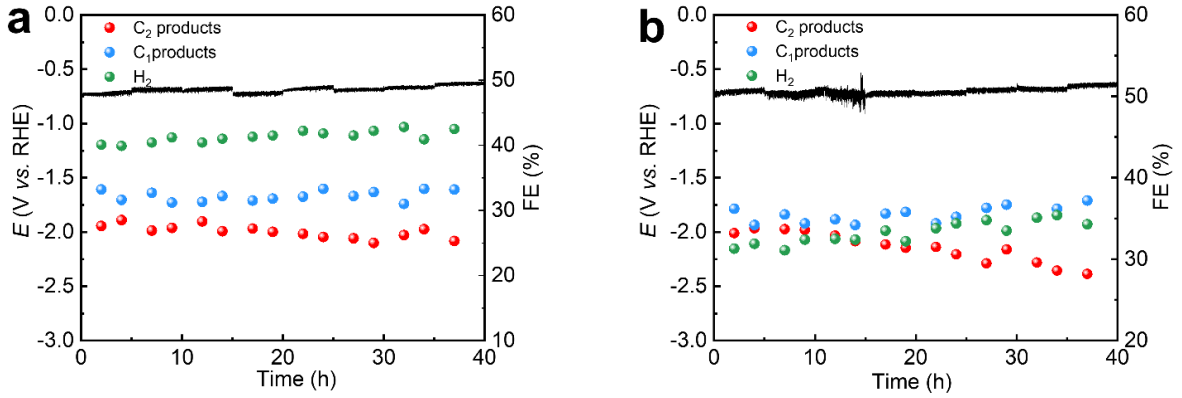

Figure S17. Long-term stability of (a) R-Cu_1/Cu_{NP} at a constant current density of 200 mA cm^{-2} and (b) P-Cu_1/Cu_{NP} at a constant current density of 400 mA cm^{-2} in 5 M KOH electrolyte (the electrode was washed, then dried and the electrolyte was refreshed at intervals 5 h to address the issues of flooding and carbonation).

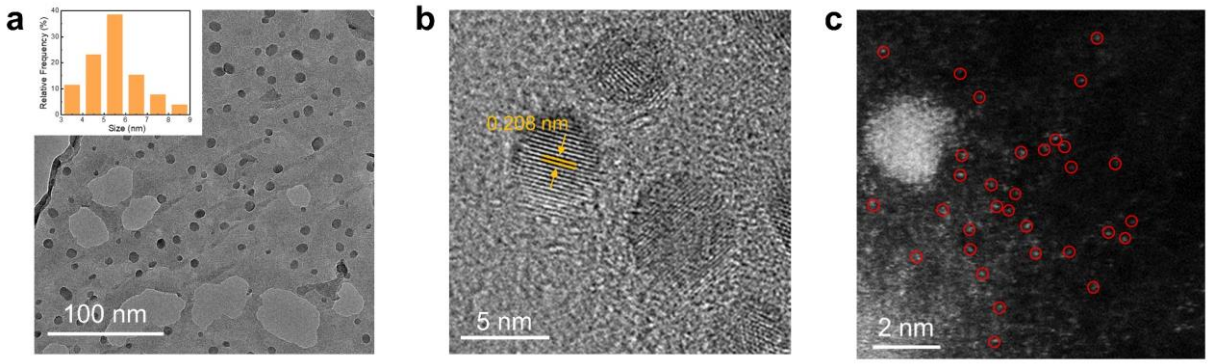

Figure S18. (a) TEM image (inset shows particle size distribution), (b) HRTEM image and (c) aberration-corrected HAADF-STEM image of M-Cu_1/Cu_{NP} after 40 h electrolysis.

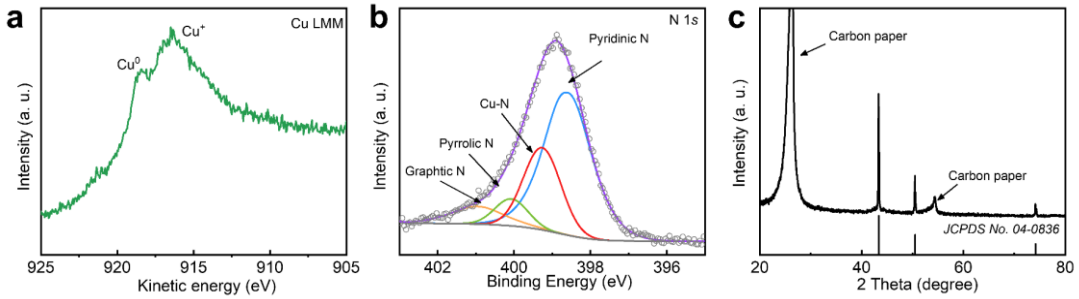

Figure S19. (a) Cu Auger LMM spectrum (b) XPS spectra of N *1s* orbits and (c) XRD pattern of M-Cu_1/Cu_{NP} after 40 h electrolysis.

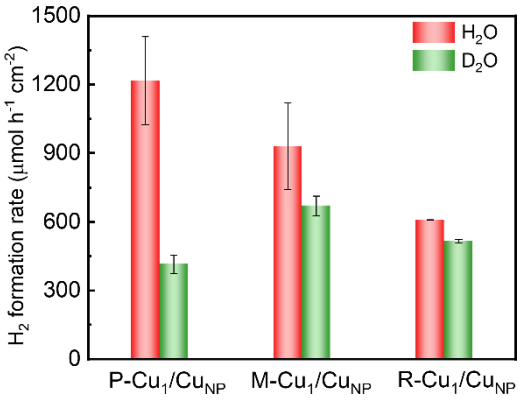

Figure S20. The kinetic isotope effect of H_2O/D_2O on P-Cu_1/Cu_{NP} M-Cu_1/Cu_{NP} and R-Cu_1/Cu_{NP} at -0.6 V in flow cell with 5 M KOH electrolyte. Values are means and error bars indicate s.d. (n = 3 replicates).

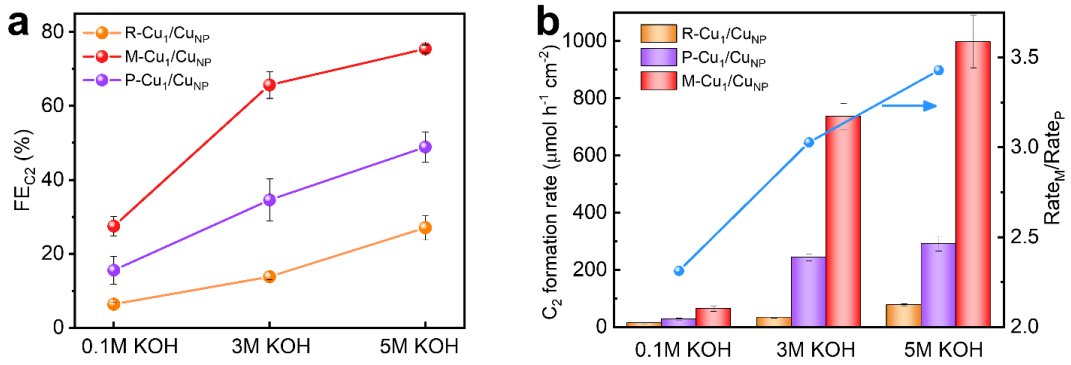

Figure S21. (a) FE_{C2} of R-Cu_1/Cu_{NP},M-Cu_1/Cu_{NP} and P-Cu_1/Cu_{NP} in different concentrations KOH electrolyte at -0.6 V. (b) C_2 formation rate of R-Cu_1/Cu_{NP},M-Cu_1/Cu_{NP} and P-Cu_1/Cu_{NP} in different concentrations KOH electrolyte at -0.6 V and $Rate_M/Rate_P$ of M-Cu_1/Cu_{NP} to P-Cu_1/Cu_{NP}. Values are means and error bars indicate s.d. (*n* = 3 replicates).

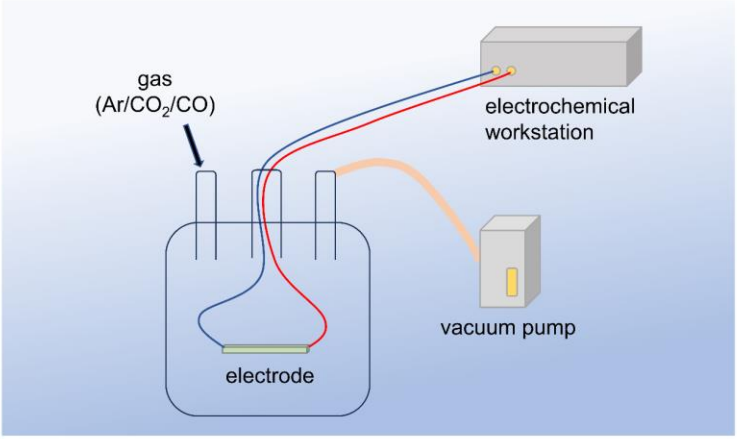

Figure S22. The device scheme of gas electro-response experiments.

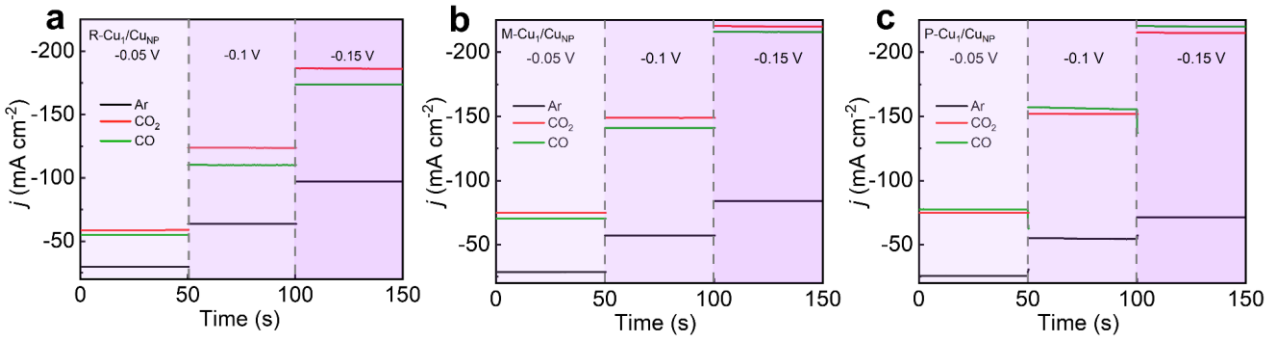

Figure S23. The CO_2 and CO gas adsorption electroresponse current density of (a) R-Cu_1/Cu_{NP}, (b) M-Cu_1/Cu_{NP} and (c) P-Cu_1/Cu_{NP}.

The capacity adsorption of CO_2 and CO molecules on the catalysts surface was tested by a self-desined gas adsorption electroresponse device. The Cu foam sprayed with the catalyst was used as electrode. The as-prepared electrode was placed in a sealed container and connected with the electrochemical workstation. Various gas (CO_2、CO and Ar) were injected into the container and the curve of current was monitored under different applied potentials (-0.05, -0.1 and -0.15 V).

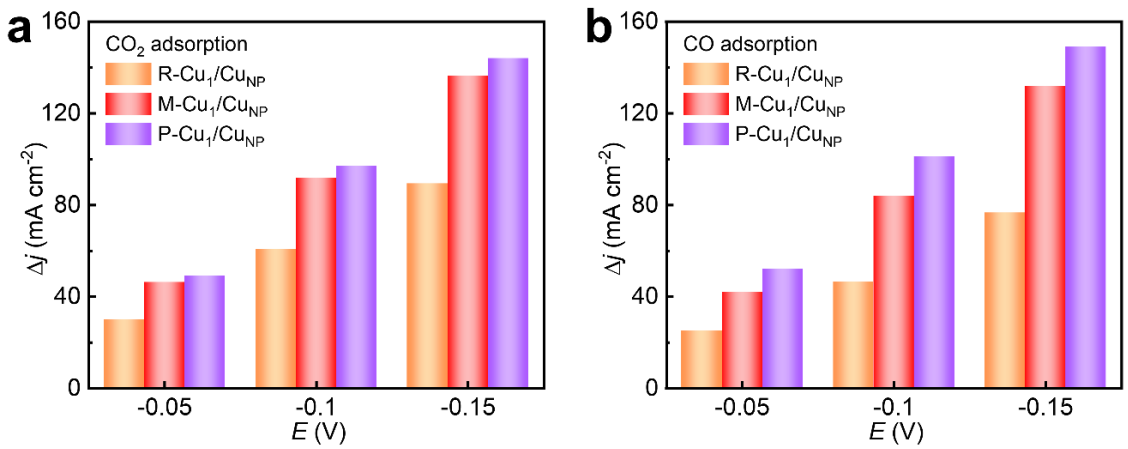

Figure S24. Results of (a) CO_2 and (b) CO adsorption responses under different applied voltages over R-Cu_1/Cu_{NP}, M-Cu_1/Cu_{NP} and P-Cu_1/Cu_{NP}.

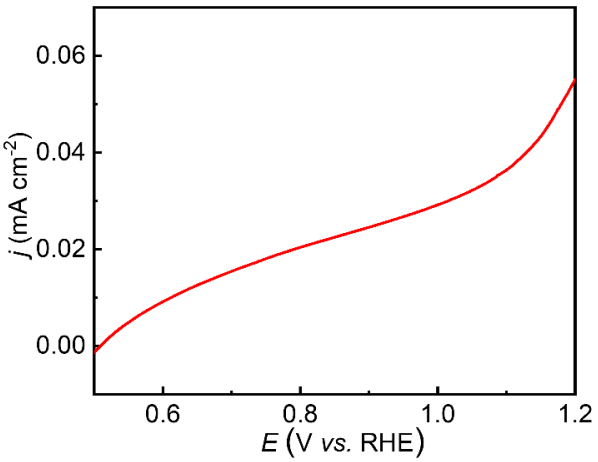

Figure S25. The LSV cruve of M-Cu_1/Cu_{NP} in 0.1 M Na_2SO_4 aqueous solution without CO adsorption.

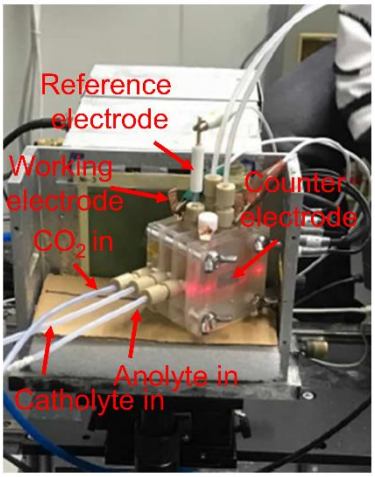

Figure S26. The optical photo of flow cell used for *in situ* XAS experiment.

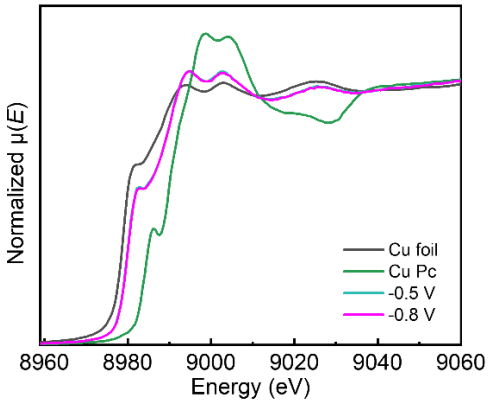

Figure S27. The *in situ* XANES spectra at Cu K-edge over M-Cu_1/Cu_{NP} at -0.5 and -0.8 V in 5 M KOH electrolyte.

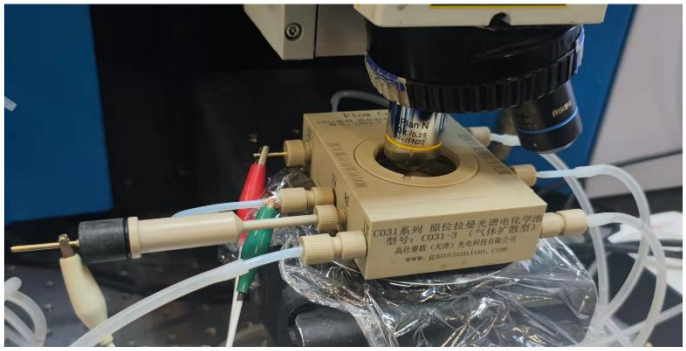

Figure S28. The photograph of cell used for *in situ* SERS spectroscopy.

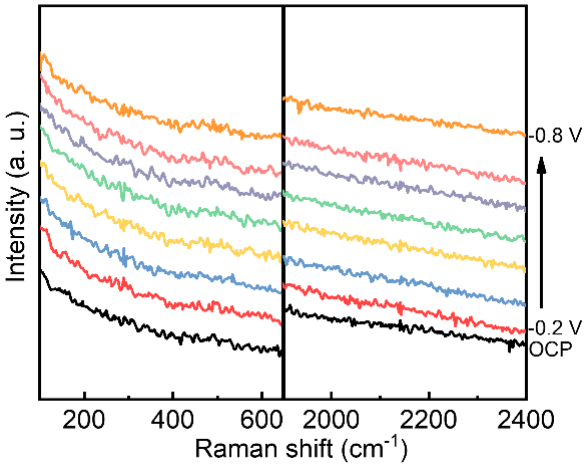

Figure S29. *In situ* surface-enhanced Raman spectra recorded at different applied potentials for Cu-N-C during CO_2RR.

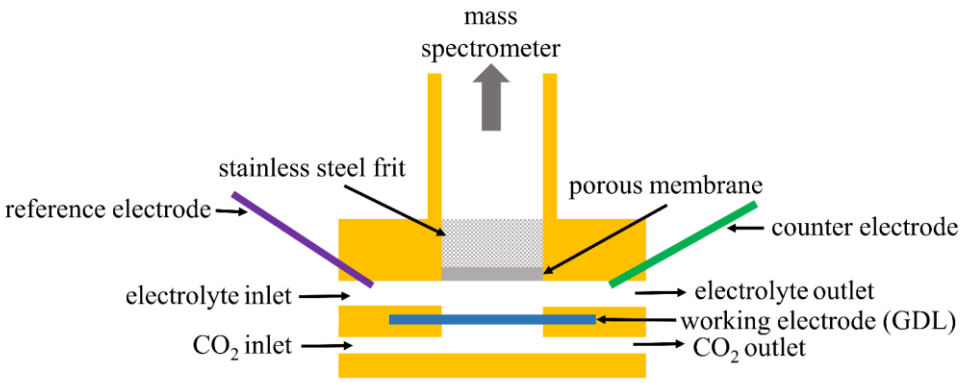

Figure S30. The scheme of cell used for online DEMS measurements.

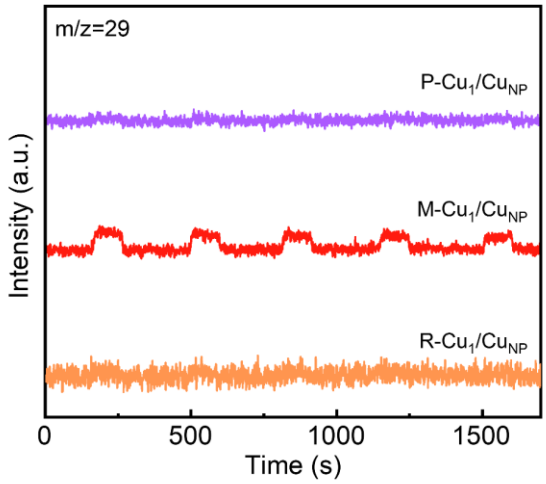

Figure S31. The m/z signal of 29 of P-Cu_1/Cu_{NP}, M-Cu_1/Cu_{NP} and R-Cu_1/Cu_{NP} during online DEMS measurements for CO_2RR at -0.6 V in five continuous cycles in 5 M KOH electrolyte.

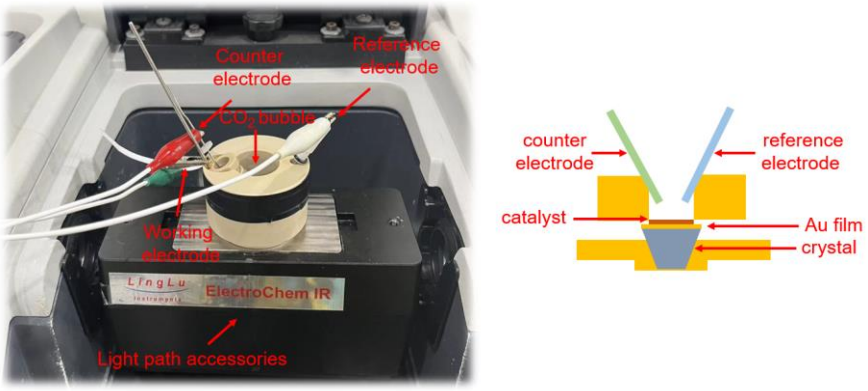

Figure S32. The photograph and scheme of cell used for *in situ* ATR-SEIRAS spectroscopy.

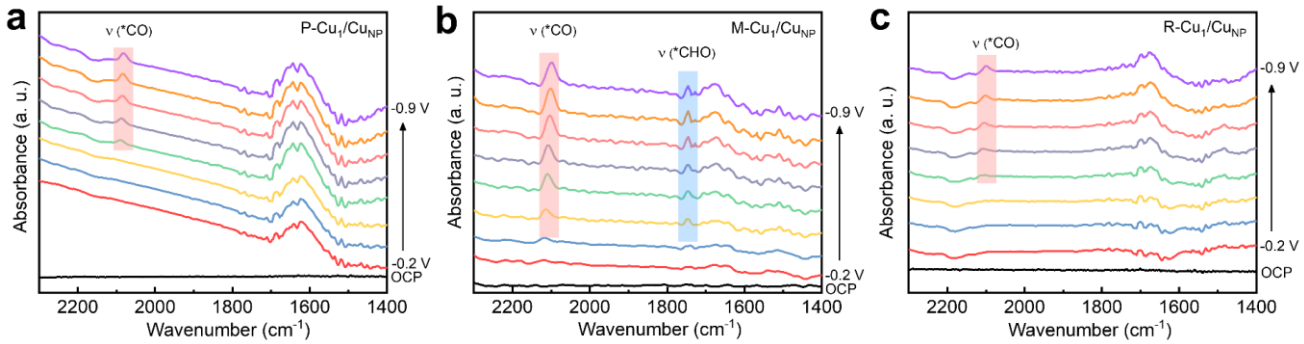

Figure S33. *In situ* ATR-SEIRAS spectra recorded at different applied potentials for (a) P-Cu_1/Cu_{NP}, (b) M-Cu_1/Cu_{NP} and (c) R-Cu_1/Cu_{NP} during CO_2RR in CO_2-saturated 3 M KOH electrolyte.

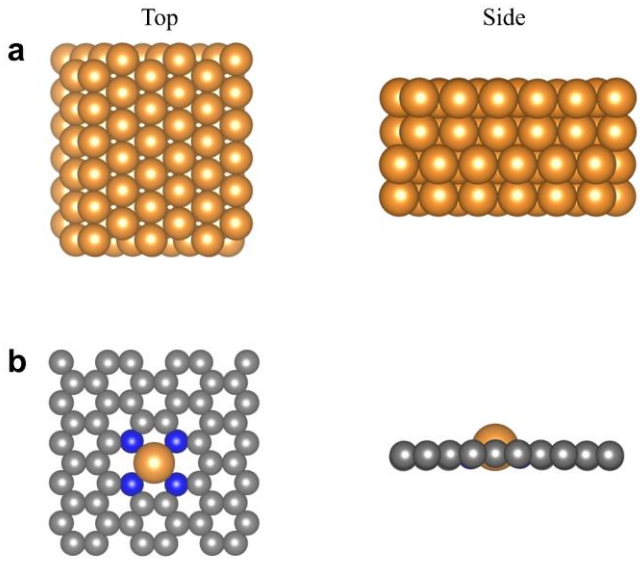

Figure S34. The top and side views of (a) Cu(111) and (b) Cu-N_4 models.

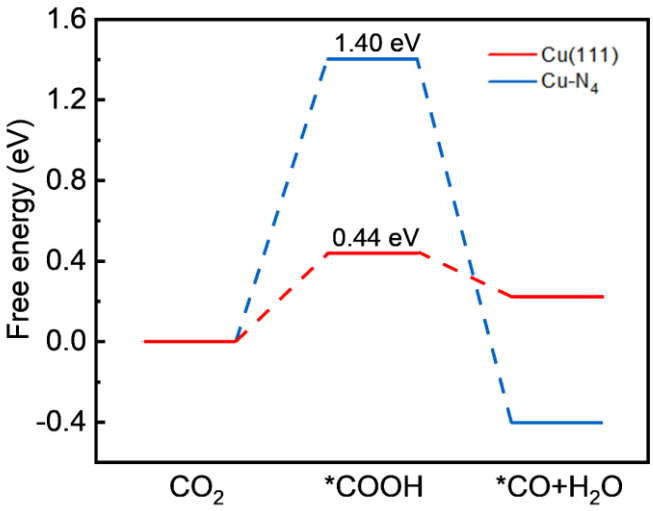

Figure S35. The free energy diagram for CO_2RR to describe the activation of CO_2 over Cu(111) and Cu-N_4.

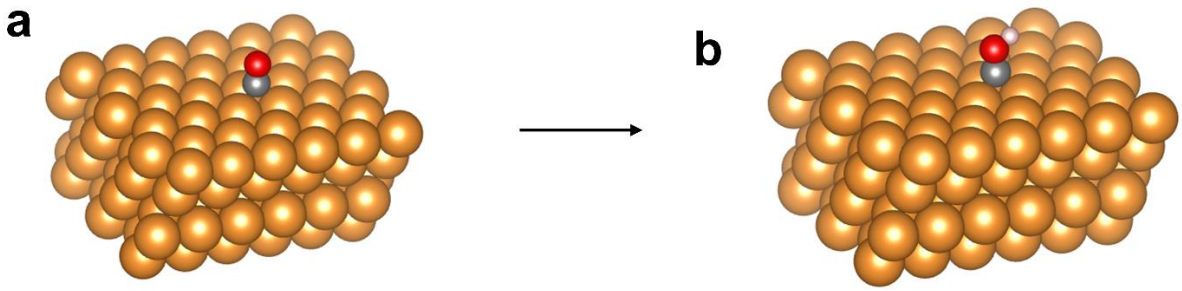

Figure S36. Side views of (a) *CO and (b) *COH on the Cu(111) facet.

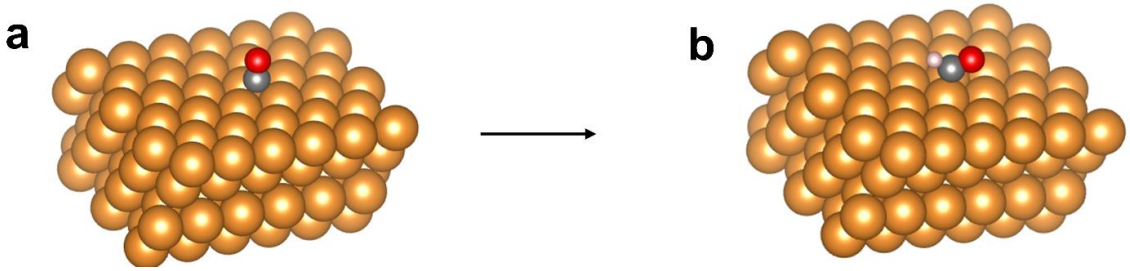

Figure S37. Side views of (a) *CO and (b) *CHO on the Cu(111) facet.

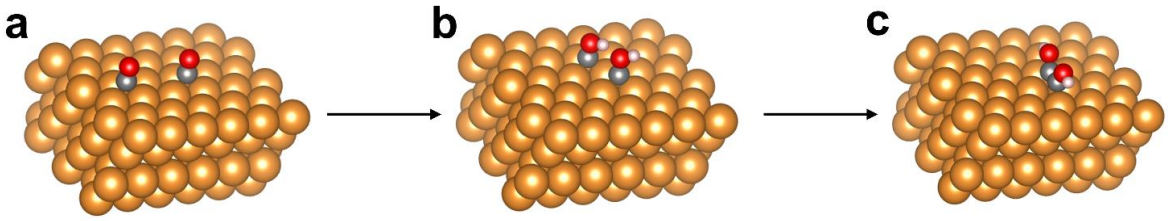

Figure S38. Side views of (a) *CO-*CO, (b) *COH-*COH and (c) *COH*COH on the Cu(111) facet.

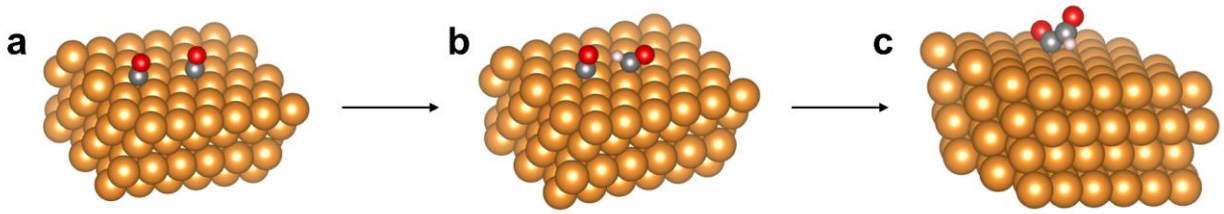

Figure S39. Side views of (a) *CO-*CO, (b) *CO-*CHO and (c) O*CCHO on the Cu(111) facet.

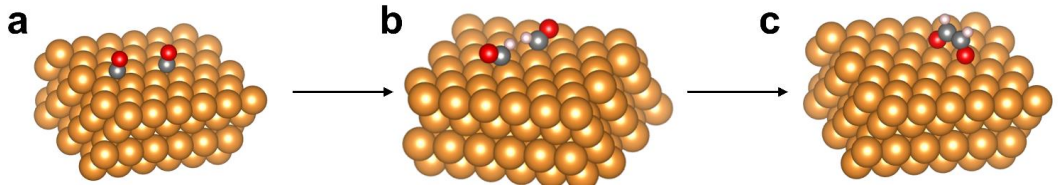

Figure S40. Side views of (a) *CO-*CO, (b) *CHO-*CHO and (c) *OHCCHO* on the Cu(111) facet.

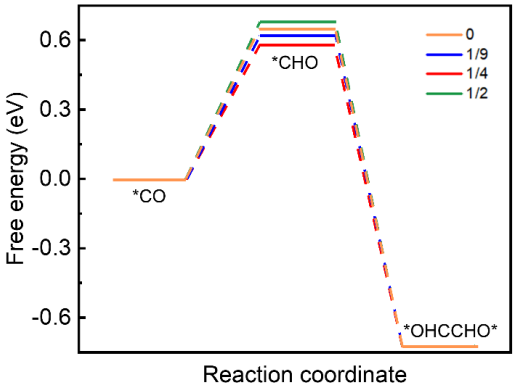

Figure S41. Free energy of *CO hydrogenation to *CHO on Cu(111) under different *H coverage.

Table S1. The contents of Cu, N and C of the catalysts measured by XPS

Sample	Cu at%	N at%	C at%
P-Cu_1/Cu_{NP}	7.4	33.5	59.1
M-Cu_1/Cu_{NP}	4.3	40.5	55.2
R-Cu_1/Cu_{NP}	1.9	47.2	50.9

Table S2. Structural parameters extracted from the EXAFS fitting. (S_0^2=0.80)

Sample	Scattering pair	CN_{real}	R(Å)	$\sigma^2(10^{-3}Å^2)$	ΔE_0(eV)	P (%)
R-Cu_1/Cu_{NP}	Cu-N	3.9	1.96	5.8	-3.5	28 (Cu_1)
	Cu-Cu	8.6	2.56*	4.9	2.1	72 (Cu_{NP})
M-Cu_1/Cu_{NP}	Cu-N	3.8	1.96	5.1	-3.4	20 (Cu_1)
	Cu-Cu	8.6	2.56*	5.4	2.1	80 (Cu_{NP})
P-Cu_1/Cu_{NP}	Cu-N	0.4	1.96	6.0	-3.5	5 (Cu_1)
	Cu-Cu	8.4	2.56*	4.8	2.1	95 (Cu_{NP})
Cu-N-C	Cu-N	4.0	1.96	5.9	-3.5	-

S_0^2 is the amplitude reduction factor S_0^2=0.8; CN_{real} is the coordination number; R is interatomic distance (the bond length between central atoms and surrounding coordination atoms); σ^2 is Debye-Waller factor (a measure of thermal and static disorder in absorber-scatterer distances); ΔE_0 is edge-energy shift (the difference between the zero kinetic energy value of the sample and that of the theoretical model). R factor is used to value the goodness of the fitting. * represents a fixed value for the parameter. P represents the percentage of Cu-N_4 (Cu_1) and Cu NPs Cu in total Cu species of catalyst.

Table S3. Product FEs, total current density and error bar of R-Cu_1/Cu_{NP} at various potentials in 5 M KOH electrolyte.

Potential (V)	C_2H_5OH FE (%)			Error bar
-0.4	0.0	0.0	0.0	0.00
-0.5	0.0	0.0	0.0	0.00
-0.6	14.8	11.3	7.0	3.90
-0.7	17.2	21.6	19.2	2.20
-0.8	9.0	11.7	6.4	2.65
-0.9	6.3	7.1	7.5	0.61

Potential (V)	CH_3COOH FE (%)			Error bar
-0.4	0.0	0.0	0.0	0.00
-0.5	0.0	0.0	0.0	0.00
-0.6	5.5	8.2	6.8	1.35
-0.7	12.7	12.0	13.7	0.85
-0.8	3.8	5.7	4.7	0.95
-0.9	2.8	3.3	3.7	0.45

Potential (V)	C_2H_4 FE (%)			Error bar
-0.4	0.0	0.0	0.0	0.00
-0.5	7.6	7.7	7.9	0.15
-0.6	9.1	9.5	9.2	0.21
-0.7	9.6	8.5	10.6	1.05
-0.8	4.8	4.5	4.5	0.17
-0.9	3.2	4.4	4.0	0.61

Potential (V)	HCOOH FE (%)			Error bar
-0.4	0.0	0.0	0.0	0.00
-0.5	17.4	17.1	16.4	0.51
-0.6	4.1	6.7	5.5	1.30
-0.7	2.7	2.1	3.0	0.46
-0.8	0.5	0.7	0.6	0.10
-0.9	0.5	0.6	0.7	0.10

Potential (V)	CO FE (%)			Error bar
-0.4	22.3	23.1	21.4	0.85
-0.5	23.1	22.8	23	0.15
-0.6	7.9	10.8	9.2	1.45
-0.7	4	4.5	5.1	0.55
-0.8	0.8	1.8	1.2	0.50
-0.9	1.2	1.6	0.9	0.35

Potential (V)	CH_4 FE (%)			Error bar
-0.4	0.0	0.0	0.0	0.00
-0.5	2.8	2.2	2.4	0.31
-0.6	19.4	18.6	20.0	0.70
-0.7	22.6	24.0	22.9	0.74
-0.8	17.8	21.3	20.0	1.77
-0.9	13.7	20.5	17.5	3.41

Potential (V)	H_2 FE (%)			Error bar
-0.4	71.8	73.7	74.0	1.19
-0.5	51.1	52.7	52.1	0.81
-0.6	40.2	39.5	40.1	0.38
-0.7	30.9	28.5	26.6	2.15
-0.8	64.8	54.2	59.8	5.30
-0.9	76.4	64.0	70.5	6.20

Potential (V)	Total current density (mA cm^{-2})			Error bar
-0.4	5.7	6.2	6.0	0.25
-0.5	21.3	22.9	19.8	1.55
-0.6	81.1	82.3	81.5	0.60
-0.7	191.0	187.0	189.0	2.00
-0.8	493.2	487.0	497.2	5.14
-0.9	798.0	787.0	792.0	5.51

Table S4. Product FEs, total current density and error bar of M-Cu_1/Cu_{NP} at various potentials in 5 M KOH electrolyte.

Potential (V)	C_2H_5OH FE (%)			Error bar
-0.4	0	0	0	0
-0.5	10.8	15.3	14	2.30
-0.6	30.1	29.2	29	0.59
-0.7	27	28	28	0.58
-0.8	24.1	23.9	23.6	0.25
-0.9	19.6	19.9	19	0.46

Potential (V)	CH_3COOH FE (%)			Error bar
-0.4	12.7	13.1	10.9	1.17
-0.5	18.3	11.8	18	3.67
-0.6	15.5	14.4	20	2.97
-0.7	17.7	16.7	15.3	1.21
-0.8	11.8	13.1	10	1.56
-0.9	7.2	6.3	6.5	0.47

Potential (V)	C_2H_4 FE (%)			Error bar
-0.4	6.9	7.3	10.5	1.97
-0.5	17.6	17.9	20.5	1.59
-0.6	29.8	30.8	27.5	1.69
-0.7	26.7	25.7	25.4	0.68
-0.8	22.1	23.9	22.9	0.90
-0.9	22.6	20.4	19.7	1.51

Potential (V)	HCOOH FE (%)			Error bar
-0.4	8.6	8.9	9.2	0.30
-0.5	12.5	7.5	7.9	2.78
-0.6	2.4	3.1	2.5	0.38
-0.7	3.5	2.2	2.3	0.72
-0.8	1.5	2.1	1.5	0.35
-0.9	1.2	2.7	3.2	1.04

Potential (V)	CO FE (%)			Error bar
-0.4	35.3	35.6	30.4	2.92
-0.5	23.7	27.8	22.4	2.82
-0.6	10.1	11.3	10.7	0.60
-0.7	7.4	5.4	5.3	1.18
-0.8	3.2	3.4	4.7	0.81
-0.9	4.1	3.6	4.5	0.45

Potential (V)	CH_4 FE (%)			Error bar
-0.4	0	0	0	0.00
-0.5	1.6	1.3	1.9	0.30
-0.6	2.2	1.7	4.5	1.49
-0.7	2.9	7.3	5.3	2.20
-0.8	4.9	5.8	7.6	1.37
-0.9	4.5	3.7	2.2	1.17

Potential (V)	H_2 FE (%)			Error bar
-0.4	37.4	39.8	41.8	2.20
-0.5	18.3	20.9	17.8	1.66
-0.6	11.1	11.3	17.0	3.35
-0.7	17.3	17.7	22.6	2.95
-0.8	33.8	27.9	31.7	2.99
-0.9	42.8	46	45.3	1.68

Potential (V)	Total current density (mA cm^{-2})			Error bar
-0.4	58.4	49.5	56.5	4.69
-0.5	166.8	163.6	140	14.64
-0.6	426	365.5	358.7	37.05
-0.7	635.2	650.5	663.5	14.17
-0.8	895.6	913.5	892.7	11.27
-0.9	1211.83	1212.3	1198.8	7.66

Table S5. Product FEs, total current density and error bar of P-Cu_1/Cu_{NP} at various potentials in 5 M KOH electrolyte.

Potential (V)	C_2H_5OH FE (%)			Error bar
-0.4	0.0	0.0	0.0	0.00
-0.5	0.0	0.0	0.0	0.00
-0.6	13.4	12.3	12.6	0.57
-0.7	14.2	16.0	15.2	0.90
-0.8	14.5	13.1	11.6	1.45
-0.9	12.2	10.2	13.9	1.85

Potential (V)	CH_3COOH FE (%)			Error bar
-0.4	0.0	0.0	0.0	0.00
-0.5	3.5	3.9	3.2	0.35
-0.6	4.0	4.5	5.1	0.55
-0.7	10.0	10.1	10.3	0.15
-0.8	8.0	7.2	7.5	0.40
-0.9	8.3	6.7	9.9	1.60

Potential (V)	C_2H_4 FE (%)			Error bar
-0.4	0.0	0.0	0.0	0.00
-0.5	3.1	2.9	3.5	0.31
-0.6	16.2	17.2	14.5	1.37
-0.7	21.1	24.7	20.3	2.34
-0.8	23.0	23.2	24.0	0.53
-0.9	27.8	23.9	22.9	2.59

Potential (V)	HCOOH FE (%)			Error bar
-0.4	42.0	45.0	44.0	1.53
-0.5	30.1	32.2	31.0	1.05
-0.6	13.4	14.6	15.0	0.83
-0.7	5.7	5.7	5.7	0.00
-0.8	5.7	3.9	4.5	0.92
-0.9	4.2	4.5	4.0	0.25

Potential (V)	CO FE (%)			Error bar
-0.4	10.6	11.4	13.0	1.22
-0.5	16.9	14.1	17.0	1.65
-0.6	16.9	17.0	20.4	1.99
-0.7	16.5	13.2	14.7	1.65
-0.8	12.0	11.1	13.5	1.21
-0.9	11.6	10.8	12.2	0.70

Potential (V)	CH_4 FE (%)			Error bar
-0.4	0.0	0.0	0.0	0.00
-0.5	1.0	1.2	1.4	0.20
-0.6	4.5	3.1	3.4	0.74
-0.7	5.9	5.1	6.2	0.57
-0.8	4.5	5.5	5.5	0.58
-0.9	6.7	6.6	6.5	0.10

Potential (V)	H_2 FE (%)			Error bar
-0.4	45.6	43.1	44.0	1.27
-0.5	48.1	53.1	51.1	2.52
-0.6	30.5	28.2	37.1	4.62
-0.7	28.4	28.0	28.5	0.26
-0.8	31.5	33.7	35.8	2.15
-0.9	40.4	38.1	40.5	1.36

Potential (V)	Total current density (mA cm^{-2})			Error bar
-0.4	21.2	19.8	20.4	0.70
-0.5	83.4	85.9	84.3	1.27
-0.6	211.2	196.0	204.5	7.62
-0.7	367.0	365.7	370.0	2.21
-0.8	554.0	598.3	573.2	22.22
-0.9	860.1	860.0	852.0	4.65

Table S6. Product FEs, total current density and error bar of Cu-N-C at various potentials in 5 M KOH electrolyte.

Potential (V)	CO FE (%)			Error bar
-0.4	0	0	0	0
-0.5	3.1	2.7	2.5	0.30
-0.6	2.4	3.4	2.4	0.57
-0.7	2	3.5	2	0.86
-0.8	1.3	3.2	1.4	1.06
-0.9	0	1.8	0	1.03

Potential (V)	CH_4 FE (%)			Error bar
-0.4	0	0	0	0.00
-0.5	2.7	4.3	4.4	0.95
-0.6	2.1	7.8	4.4	2.87
-0.7	3.2	8.8	3.8	3.07
-0.8	1.4	8.6	2.7	3.84
-0.9	0	1.4	1.2	0.76

Potential (V)	H_2 FE (%)			Error bar
-0.4	98.1	98.2	98.5	0.21
-0.5	93.8	92.0	94.2	1.17
-0.6	95.1	87.8	93.3	3.80
-0.7	95.4	87.9	92.1	3.76
-0.8	98.4	87.4	95.7	5.73
-0.9	99.8	97.6	98.3	1.12

Potential (V)	Total current density (mA cm^{-2})			Error bar
-0.4	33.3	32.6	27.9	2.95
-0.5	81.1	64.7	73.7	8.19
-0.6	114.3	99.0	101.8	8.14
-0.7	153.2	136.4	149.4	8.82
-0.8	196.2	168.2	187.0	14.26
-0.9	249.2	228.3	241.0	10.52

Table S7. Performance comparison of various catalysts for CO_2 electroreduction to C_{2+} products.

Samples	E (V *vs.* RHE)	FE_{C2+} (%)	j_{C2+} (mA cm^{-2})	References
M-Cu_1/Cu_{NP}	-0.60	75.4	289.2	This work
Nanoporous Cu	-0.67	62.0	404.8	1
Reconstructed Cu	-1.80	77.0	346.5	2
NGQ/Cu-nr	-0.90	~74.0	~208.0	3
F-Cu	-0.89	80.0	1280.0	4
Multihollow Cu_2O	-0.61	75.0	267.0	5
CuAg wire	-0.70	85.0	255.0	6
FeTPP[Cl]/Cu	-0.82	85.0	257.0	7
OD-Cu-III	-	74.9	224.7	8
Cu dendrites	-0.68	64.0	255.0	9
Cu	-	80.4	120.6	10
Cu(0)@PIL@Cuba(I)	-0.85	76.1	304.2	11
3-shell HoMSs	-0.88	77.0	513.7	12
Cu-PTFE	-1.50	86.0	~250.0	13
CuS/Cu-V	-0.92	52.8	147.8	14
$Ce(OH)_x$-doped-Cu	-0.70	80.3	211.2	15
Cu-KI	-1.09	~72.6	29.0	16
Graphite/Cu/PTFE	-0.54	83.0	275.0	17
Polyamine-incorporated Cu	-0.47	87.0	~35.0	18

Supplementary References

1. Lv J. J. et al. A highly porous copper electrocatalyst for carbon dioxide reduction. *Adv. Mater.* **30**, 1803111 (2018).
2. Kibria M. G. et al. A surface reconstruction route to high productivity and selectivity in CO_2 electroreduction toward C_{2+} hydrocarbons. *Adv. Mater.* **30**, 1804867 (2018).
3. Chen C. et al. Highly efficient electroreduction of CO_2 to C_{2+} alcohols on heterogeneous dual active sites. *Angew. Chem. Int. Ed.* **59**, 16459-16464 (2020).
4. Ma W. et al. Electrocatalytic reduction of CO_2 to ethylene and ethanol through hydrogen-assisted C–C coupling over fluorine-modified copper. *Nat. Catal.* **3**, 478-487 (2020).
5. Yang P. P. et al. Protecting copper oxidation state via intermediate confinement for selective CO_2 electroreduction to C2+ fuels. *J. Am. Chem. Soc.* **142**, 6400-6408 (2020).
6. Hoang T. T. H. et al. Nanoporous copper-silver alloys by additive-controlled electrodeposition for the selective electroreduction of CO_2 to ethylene and ethanol. *J. Am. Chem. Soc.* **140**, 5791-5797 (2018).
7. Li F. et al. Cooperative CO_2-to-ethanol conversion via enriched intermediates at molecule–metal catalyst interfaces. *Nat. Catal.* **3**, 75-82 (2019).
8. Wu Z. Z. et al. Identification of Cu(100)/Cu(111) interfaces as superior active sites for CO dimerization during CO_2 electroreduction. *J. Am. Chem. Soc.* **144**, 259-269 (2022).
9. Niu Z. Z. et al. Hierarchical copper with inherent hydrophobicity mitigates electrode flooding for high-rate CO_2 electroreduction to multicarbon products. *J. Am. Chem. Soc.* **143**, 8011-8021 (2021).
10. Zhang X. et al. Selective and high current CO_2 electro-reduction to multicarbon products in near-neutral KCl electrolytes. *J. Am. Chem. Soc.* **143**, 3245-3255 (2021).
11. Xu B. H. et al. Highly efficient electrocatalytic CO_2 reduction to C_{2+} products on a poly(ionic liquid)-based Cu(0)-Cu(I) tandem catalyst. *Angew. Chem. Int. Ed.* **61**, e202110657 (2021).
12. Liu C. et al. Nanoconfinement engineering over hollow multi-shell structured copper towards efficient electrocatalytical C-C coupling. *Angew. Chem. Int. Ed.* **61**, e202113498 (2021).
13. Yang B. et al. Accelerating CO_2 electroreduction to multicarbon products via synergistic electric-thermal field on copper nanoneedles. *J. Am. Chem. Soc.* **144**, 3039-3049 (2022).
14. Zhuang T.-T. et al. Steering post-C–C coupling selectivity enables high efficiency electroreduction of carbon dioxide to multi-carbon alcohols. *Nat. Catal.* **1**, 421-428 (2018).
15. Luo M. et al. Hydroxide promotes carbon dioxide electroreduction to ethanol on copper via tuning of adsorbed hydrogen. *Nat. Commun.* **10**, 5814 (2019).
16. Kim T. et al. A scalable method for preparing Cu electrocatalysts that convert CO_2 into C_{2+} products. *Nat. Commun.* **11**, 3622 (2020).
17. Dinh C.-T. et al. CO_2 electroreduction to ethylene via hydroxide-mediated copper catalysis at an abrupt interface. *Science* **360**, 783-787 (2018).
18. Chen X. et al. Electrochemical CO_2-to-ethylene conversion on polyamine-incorporated Cu electrodes. *Nat. Catal.* **4**, 20-27 (2020).